Available online at www.sciencedirect.com

SciVerse ScienceDirect

Journal of the European Ceramic Society 32 (2012) 1847–1854

www.elsevier.com/locate/jeurceramsoc

Anisotropic thermal conductivity of silicon nitride ceramics containing carbon nanostructures

Pilar Miranzo *, Eugenio García, Cristina Ramírez, Jesús González-Julián, Manuel Belmonte, M. Isabel Osendi

Instituto de Cerámica y Vidrio, ICV-CSIC, C/Kelsen 5, Cantoblanco, 28049 Madrid, Spain

Received 10 October 2011; received in revised form 16 January 2012; accepted 18 January 2012
Available online 16 February 2012

Abstract

Silicon nitride (Si_3N_4) composites containing carbon nanotubes (CNTs) or graphene nanoplateles (GNPs) are of great relevance in the electronic and aerospace industries where the search for new materials with enhanced and anisotropic thermal conductivity to work in harsh environments is a strategic guideline. Here we study thermal conduction in Si_3N_4 composites with different amounts of carbon nanostructures. The effects of the nanostructure orientation respect the heat flux, the testing temperature and the α/β Si_3N_4 phase ratio are analyzed. The addition of CNTs and GNPs leads to an anisotropic thermal response, decreasing the through-thickness thermal conductivity of the Si_3N_4 composites and raising the in-plane thermal conductivity, especially for GNPs that enhance it up to twice that of the monolithic Si_3N_4. This effect is related to the preferred orientation of the nanostructures that gives a less resistive network in the in-plane direction and the intrinsic anisotropy of their thermal conductivity.

Keywords: Microstructure-final; Nanocomposites; Si_3N_4; Carbon nanostructures; Thermal conductivity

1. Introduction

The thermal conductivity (κ) of the diverse carbon allotropes, including the latest discovered carbon nanostructures (C-n), extents over an extraordinary wide range of values, from the very low figures of amorphous carbon to the peak value reported for graphene and carbon nanotubes (CNTs). Unusual large κ values have been theoretically predicted for two dimensional and one dimensional carbon crystals, but experimental results are sometimes contradictory as discussed in a recent review.[1]

Early studies on millimeter sized CNTs mats[2–6] gave relatively low κ values, 5–30 W m^{-1} K^{-1}, but they lacked to provide absolute values for single CNTs as the numerous tube–tube junctions and intrinsic defects within nanotubes became the dominant barriers to thermal transport in the mat. Consequently, to probe thermal transport free from interactions, microfabricated suspended devices with both multi-walled (MWCNTs) or single-walled (SWCNTs) nanotubes were developed.[7–10] These measurements reported a wide range of room temperature κ values for individual CNTs, although commonly quoted values were ~3000 and ~3500 W m^{-1} K^{-1} for MWCNTs and SWCNTs, respectively. Both values were well above the bulk-graphite limit but in the order of the theoretical predictions.[1] From these studies, a phonon mean free path at room temperature (Λ) of ~700–750 nm was calculated, which is shorter than the typical length for CNTs (>2 μm), meaning that the phonon transport is still diffusive but close to the ballistic transition. Furthermore, κ for MWCNT decreased with the size of MWCNT bundles, becoming, for 200 nm, similar to the bulk measurement on a mat sample, which infers that the interactions of phonons between multi-walled layers also affected thermal conduction.[10]

Recently, experimental studies done on large-area suspended graphene layers attained κ values exceeding 3000 W m^{-1} K^{-1} near room temperature.[1] The evolution of the thermal properties of few layer graphene has been examined as a function of the number of atomic planes (n), showing that κ decreases with n, even dropping below the bulk graphite limit for $n > 4$ due to the onset of the phonon-boundary scattering from the top and bottom interfaces; but the graphite value was recovered for thicker films.[11] This $\kappa(n)$ dependence agrees with current non-equilibrium molecular dynamics calculations for graphene nanoribbons.[12]

* Corresponding author. Tel.: +34 917355872; fax: +34 917355843.
E-mail address: pmiranzo@icv.csic.es (P. Miranzo).

0955-2219/$ – see front matter © 2012 Elsevier Ltd. All rights reserved.
doi:10.1016/j.jeurceramsoc.2012.01.026

In spite of the numerous experimental and theoretical studies on thermal conductivity of C-n, relatively few works can be found on the thermal transport in composites containing these nanostructures, and ever fewer devoted to ceramic matrices. Particularly, no papers could be found on ceramics containing either graphene nanoplatelets (GNPs) or nanosheets. For CNTs, κ has been measured for various ceramic matrix composites without any conclusive result regarding the effect of the C-n.[13–25] Of all these works, only one based on SWCNTs/Al_2O_3 nanocomposites[25] investigated both the through-thickness and in-plane thermal conductivity, showing a decrease in the transverse and no changes in the in-plane thermal diffusivity with SWCNTs content.

Improved thermal conductivity has been reported in the case of low thermal conductivity matrices containing MWCNTs, like in aluminoborosilicate glass[13,14] ($16\,W\,m^{-1}\,K^{-1}$ for aligned MWCNTs versus the $1.2\,W\,m^{-1}\,K^{-1}$ of the matrix) or MWCNTs/SiO_2 composites[15,16] that showed κ values of $4.1\,W\,m^{-1}\,K^{-1}$ for 10 vol.% MWCNTs compared to $2.4\,W\,m^{-1}\,K^{-1}$ of the silica matrix. For the high thermal conductor AlN, the two found sources[17,18] gave opposite results, apparently depending on the processing method. Wang et al.[17] reported reduced thermal-conductivity for MWCNTs/AlN composites fabricated by hot pressing, which they attributed to the CNTs poor dispersion and degradation, whereas Datye et al.[18] obtained enhanced thermal conductivity for spark plasma sintered (SPS) composites prepared by direct in situ growth of MWCNTs on AlN powders. Contradictory results were also found for MWCNTs/Al_2O_3 composites as both thermal conductivity decrease[19] and notably enhanced thermal properties[20] were reported, although in the later case, the CNTs were directly grown on Al_2O_3 powders by chemical vapor deposition and, therefore, the possible effect of the residual metallic catalysts cannot be disregarded.

As the properties of Si_3N_4 ceramics are strongly affected by the development of large elongated β grains, special attention should be paid to the α/β phase ratio when comparing the thermal properties of different Si_3N_4 materials.[26] Present authors[22] already reported a reduced thermal conductivity for Si_3N_4 composites with 5.3 vol.% of MWCNTs densified using SPS and, in a similar way, Corral et al.[23] observed a 62% decrease in the room temperature thermal conductivity over the monolithic material for a composite with just 2 vol.% of SWCNTs. One work claimed improved thermal conductivity for Si_3N_4 composites containing nanotubes but without giving a precise account of the β-phase content.[24]

Under this perspective, the aim of the paper is to deeply analyze thermal conduction in Si_3N_4 with different types of C-n. The effect of both CNTs and GNPs is presented and evaluated as a function of the C-n content, their possible orientation respect the heat flux, testing temperature and α/β Si_3N_4 phase ratio. The final objective is to extract the real effect of the C-n over the composites and to compare the effectiveness of the CNTs and GNPs in raising thermal conduction. Additionally, these kind of composites have shown extraordinary electrical[27,28] and tribological[29,30] responses, which make them interesting for engine components and MEMs, being suitable for electro-discharging machining, as well.[31]

2. Materials and methods

The preparation of the Si_3N_4 monolithic materials and composites containing different C-n is described elsewhere.[22,28] In short, ceramic matrix powders of composition 93 wt.% of α-Si_3N_4 (SN-E10, UBE Industries, Japan) plus 5 wt.% of Y_2O_3 (HC-Starck) and 2 wt.% of Al_2O_3 (SM8, Baikowski Chimie, France), as sintering aids, were attrition milled in isopropanol media. CVD synthesized MWCNTs of 30 nm diameter and 1–5 μm length (Nanolab Inc., USA) in concentrations ranging from 0.9 to 8.6 vol.%, and GNPs of nominally 200 nm diameter and 1 nm thickness (Angstron Materials LLC, USA) in concentrations ranging from 4.3 to 24.4 vol.%, were used for preparing the composites. The nanostructures were thoroughly mixed in alcohol media with the matrix powder suspension. The compositions were spark plasma sintered (Dr. Sinter, SPS-510CE, Japan) for 5 min in vacuum (6 Pa), applying a pressure of 50 MPa, at temperatures within the intervals 1600–1700 °C for the monolithic materials, 1585–1600 °C for the MWCNTs composites, and 1600–1625 °C for the GNPs composites. Sintered specimens were discs of 20 mm diameter and about 3 mm of thickness. All specimens showed densities (ρ), measured by water immersion, above 99% of the theoretical, with good C-n dispersion and no evidence of C-n degradation.

The β-Si_3N_4 phase content was determined by X-ray diffraction (XRD, Bruker D5000, Siemens, Germany) procedures.[32] Microstructures of the composites containing MWCNTs and GNPs were observed on fracture specimens using a field emission scanning electron microscope (FESEM, Hitachi S-4700, Japan). Transmission electron microscopy (TEM, 400 kV, Jeol JEM-4000 EX and JEOL 2000 FXII (200 kV)) was used for high magnification observation of the nanostructures. Specimens for TEM observations were prepared by sectioning, polishing, dimple grinding and ion beam milling.

Through-thickness thermal diffusivity in the direction parallel to the SPS pressing axis ($\alpha_{through}$) was measured in Ar atmosphere as a function of temperature, from 373 to 1073 K, on 8.8 mm × 8.8 mm square specimens of ~1 mm in thickness by the laser-flash method (Thermaflash 2200, Holometrix Netzsch, USA). Data are averaged over at least three measurements. No degradation occurs in the composites up to that temperature because no changes in thermal diffusivity were detected on cooling.

In-plane measurements of radial thermal diffusivity at room temperature were done using a special arrangement that fits into the equipment. In this way, heat source is confined into a circle of radius $r_0 = 2.5$ mm in the center of a large thin sample (20 mm in diameter and thickness below 1 mm), the heat flows out radially and is detected at a intermediate radius r larger than r_0 as defined by a mask of $\eta = r/r_0 = 2.2$. Thus heat detected has radial and axial components as heat flowing through the sample is blocked by the mask. The temperature rise measured at this annulus is fitted by a two-dimensional model[33] included in the software of the equipment, having as inputs the through-plane

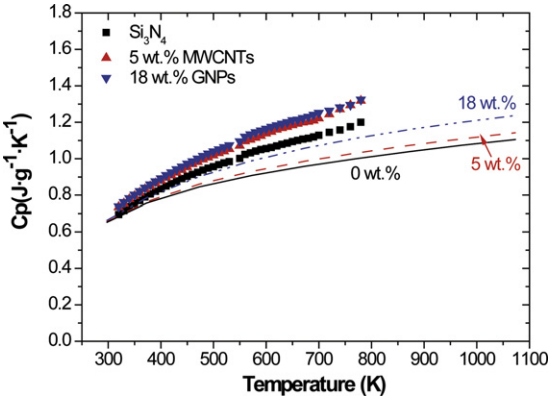

Fig. 1. Experimental values (symbols) of the specific heat as a function of temperature of three selected samples measured by DSC, and corresponding calculated values (lines) from the chemical composition and the heat capacity data of each phase.[34]

thermal diffusivity, sample thickness, r_0 and r to determine the in-plane thermal diffusivity. Data were averaged over at least 5 measurements.

The specific heat (C_p) as a function of temperature was estimated by the rule of mixtures from the chemical composition and the heat capacity data of each phase computed using the HSC Outokumpu code.[34] For the carbon nanostructures, C_p was assumed to be that of graphite as measurements were done above room temperatures.[4] As an example, C_p calculated for the monolithic (Si_3N_4 plus additives) and the composites containing 5 wt.% and 18 wt.% of C-n is plotted as a function of temperature in Fig. 1, where the C_p increase with the amount of carbon is predicted. To obtain additional experimental support of this appraisal, C_p values were measured with a differential scanning calorimeter (DSC; model: Q200, TA Instruments, USA) in the 320–873 K temperature range using a crystal of Sapphire as reference. A representative selection of specimens was chosen for the C_p experiments, namely the monolithic material, one composite with nanotubes (5 wt.% of MWCNT) and one composite containing graphene structures (18 wt.% of GNPs). The predicted increase of C_p with C-n additions was confirmed, although experimental data are always higher than the calculated ones (Fig. 1), the differences are quite reasonable for this kind of measurements. In all cases, deviations maintain within ~15%, and they are smaller (5%) for temperatures below 473 K.

Thermal conductivity (k) was then calculated from the thermal diffusivity, the density, and the calculated specific heat, using the following expression:

$$k = \alpha \cdot \rho \cdot C_p \quad (1)$$

Error bars in graphs represent the estimated accuracy of the laser flash technique, which is 7% for thermal conductivity, in the case of the through-thickness data, and the standard deviation of the values for the in-plane measurements.

In order to confirm the anisotropy in thermal conduction of MWCNTs and GNPs, similar measurements were done in commercially available buckypaper of similar nanotubes (CNP175x 225, Nanolab Inc., USA) and bulk specimens of pressed graphene nanoplatelets. In this way, discs of compressed platelets were fabricated by filling a graphite die with GNPs and applying 40 MPa of pressure at room temperature. Two types of GNPs of different sizes were used: the one used in the composite fabrication (Angstron Materials) of nominally 200 nm diameter and 1 nm thickness and larger platelets (XG sciences) with dimensions of 10 nm in thickness and 5 μm in diameter. Finally, the MWCNTs sample mat was prepared introducing four sheets of buckypaper (0.1 mm thickness) into a graphite die and spark plasma sintering at 1000 °C applying 30 MPa of pressure. These three bulk C-n specimens were thermal characterized in the through-thickness, up to 673 K, and the in-plane, at room temperature, directions.

3. Result and discussion

FESEM observations of the composites containing MWCNTs and GNPs give interesting information on their microstructure (see Fig. 2 as an example). Both C-n show a homogenous dispersion in the composites as observed on the images of the fracture surfaces, where nanotubes and nanoplatelets are seen protruding from the matrix. One particularity of the later composite that can be clearly perceived in Fig. 2b is the preferential in-plane orientation of the GNPs owing to the fabrication process, as has been previously discussed.[28] Neither MWCNTs nor GNPs are degraded after the sintering process as it was confirmed by micro-Raman spectroscopy.[22,28]

As shown in Fig. 3, the through-thickness thermal conductivity decreased with temperature in all the

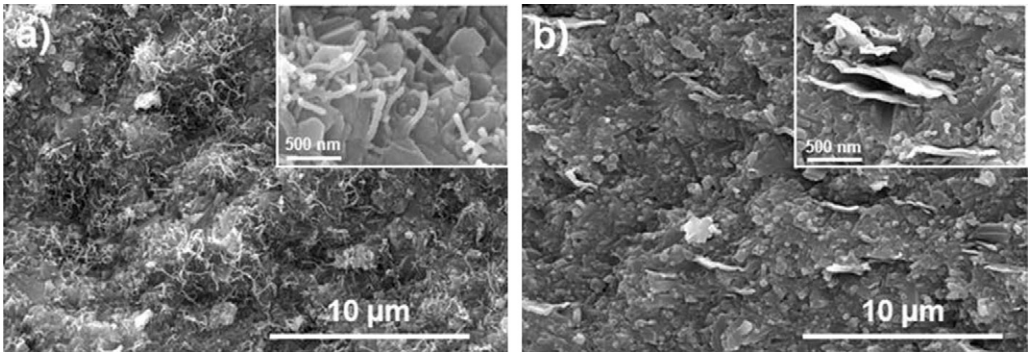

Fig. 2. FESEM micrographs of the fracture surfaces of the Si_3N_4 composites containing 3 wt.% of: (a) MWCNTs and (b) GNPs. In the right corner a detail of each microstructure is shown.

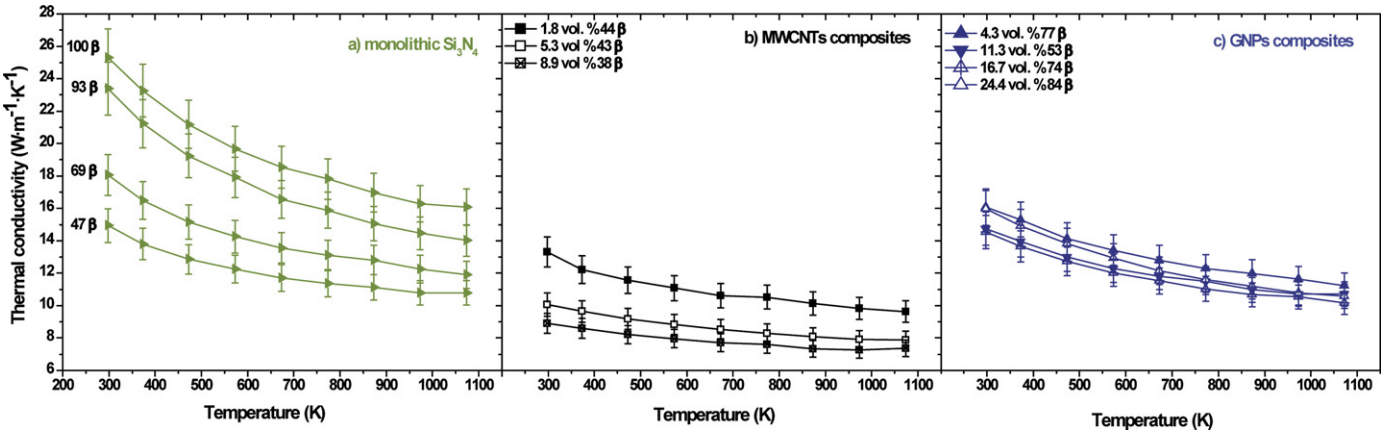

Fig. 3. Through-thickness thermal conductivity as a function of temperature for (a) monolithic Si_3N_4 materials with different amount of β-phase, (b) MWCNTs/Si_3N_4 composites and (c) GNPs/Si_3N_4 composites. The amount of C-n and the relative β-phase content in each composite are included in the legends.

materials. Independently of the presence of C-n, materials with similar κ values at room temperature (in the range 13–15 W m^{-1} K^{-1}) showed analogous temperature dependence (T^{-B}; $B = 0.25$–0.28), except for the material with 24.4 vol.% of GNPs that presented a stronger κ (T) dependence ($B = 0.33$). Monolithic materials exhibited higher κ values than materials containing C-n for equivalent phase ratios. The MWCNTs composites, with lower β-content, gave the lowest thermal conductivity values that depended on the MWCNTs content, whereas materials containing GNPs had very similar κ values for different additions.

Both the through-thickness and in-plane room temperature thermal conductivities of the monolithic Si_3N_4 materials increased with the amount of β-phase (Fig. 4), showing quasi isotropic and low κ values for β-phase contents lower than 60% ($k \sim 15$ W m^{-1} K^{-1} in both directions), whereas materials with β-phase contents $\geq$70% exhibited an increased thermal conductivity and also anisotropy, with $\kappa_{\text{in-plane}}/\kappa_{\text{through}}$ ratio of 1.25. This trend agrees with previous results on Si_3N_4 ceramics.[26,35] The increased anisotropy is associated to both the growth and orientation of the β-Si_3N_4 grains with respect to the pressing

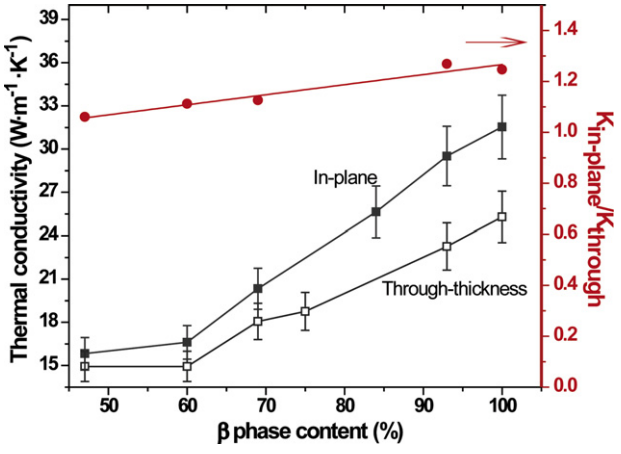

Fig. 4. In-plane and through-thickness thermal conductivity at room temperature, and the ratio between both ($\kappa_{\text{in-plane}}/\kappa_{\text{through}}$), of monolithic Si_3N_4 materials with different amount of β-phase.

direction during sintering,[36] and the intrinsic anisotropy in the thermal conductivity of the Si_3N_4 crystals.[37] The low κ values at room temperature of the present Si_3N_4 materials (lower than 28 W m^{-1} K^{-1}) are explained by the solid solution of aluminum and oxygen ions in the Si_3N_4 crystals that act as phonon scattering sites, as it has been previously reported for Al_2O_3 doped Si_3N_4.[38]

Fig. 5 shows the effect of the C-n content on the through-thickness and in-plane thermal conductivities of Si_3N_4, putting special care in comparing materials with similar β-phase content. As seen in Fig. 5a, thermal conductivity in the through-thickness direction decreases with the C-n content, but the reduction for MWCNTs is significantly stronger than for GNPs. For instance, a 3 wt.% of C-n (equivalent to 5.3 vol.% of MWCNTs and 4.3 vol.% of GNPs) led to a decrease of 33% and 11% in the thermal conductivity for MWCNTs/Si_3N_4 and GNPs/Si_3N_4, respectively. This reduction reaches 40% for the highest MWCNTs content (8.6 vol.%), whereas it is ~20% for the composite containing 16.7 vol.% of GNPs. These results indicate that thermal barriers associated to CNTs and GNPs exist for the heat flowing across the specimen, which corresponds to the SPS pressing axis direction and, in addition, that the associated thermal resistances are lower for nanoplatelets than for nanotubes. A 62% decrease in the κ at room temperature versus the monolithic material has been observed for a composite with 2 vol.% of SWCNTs,[23] whereas, in the present case, a 11% reduction is observed for a similar MWCNTs content of 1.8 vol.%. It should be mentioned that for present materials we are comparing specimens with very similar β-phase content (44 and 47%, see Figs. 3a and b).

The through-thickness κ reduction of the MWCNTs composites confirms the important role of the tube–tube junctions and intrinsic defects within nanotubes as barriers to thermal transport in ceramic composites as occurred in CNT mats.[3,5] The formation of intrinsic defects within nanotubes takes place in areas where twisting and bending occur,[39] which could reduce the phonon mean free path and affect thermal conductivity. In present materials, TEM observations indicate that MWCNTs are commonly bent and twisted at Si_3N_4 grain boundaries (Fig. 6a). In fact, Shi and Pettes[40] found that the thermal conductivity of

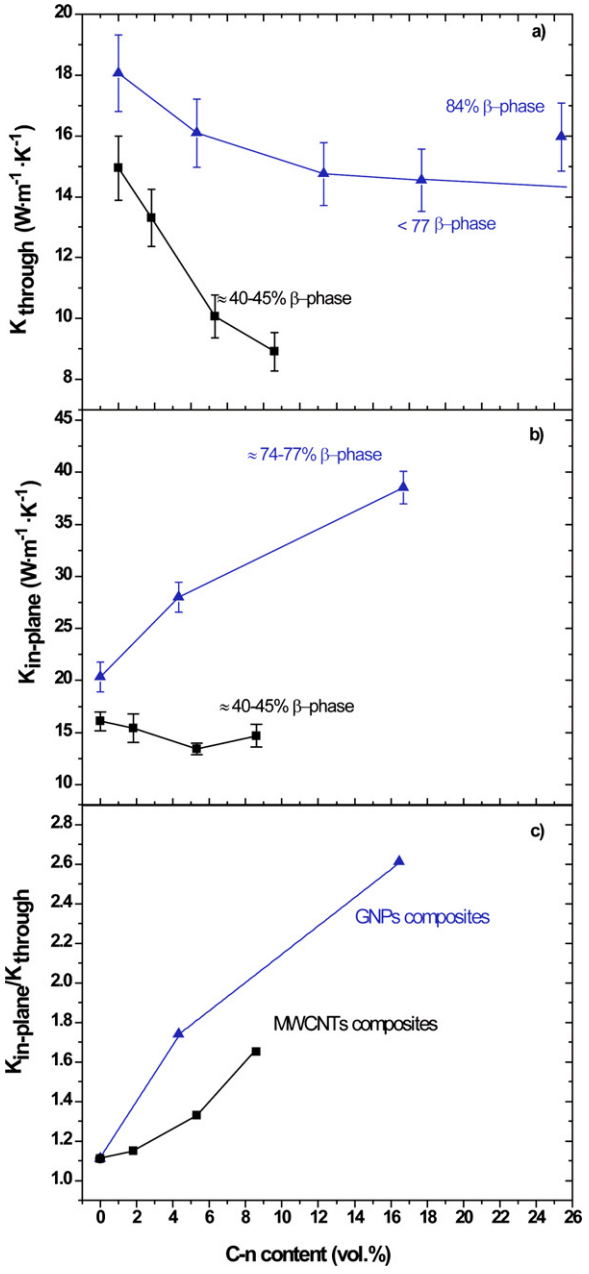

Fig. 5. Through-thickness (a) and in-plane (b) thermal conductivity at room temperature, and the $\kappa_{in\text{-}plane}/\kappa_{through}$ ratio (c), for the Si_3N_4 composites containing MWCNTs and GNPs, as a function of the C-n content. Black squares = MWCNTs and blue triangles = GNPs composites.

MWCNTs samples correlated well with the defects concentration within the nanotubes.

Regarding GNPs composites, GNP–GNP contacts and intrinsic defects within GNPs also act as barriers to thermal transport in the through-thickness direction. In fact, GNPs are also bent and twisted at the ceramic grain boundaries (Fig. 6b), which would limit the phonon mean free path. The reduction in through-thickness κ seems to be independent of the matrix β-phase content as we are comparing materials from 53 to 84% of β-Si_3N_4. Furthermore, the thermal conductivity even increases for the 24.4 vol.% of GNPs composite, which cannot be justified by the slightly higher β-phase content of this material (84%)

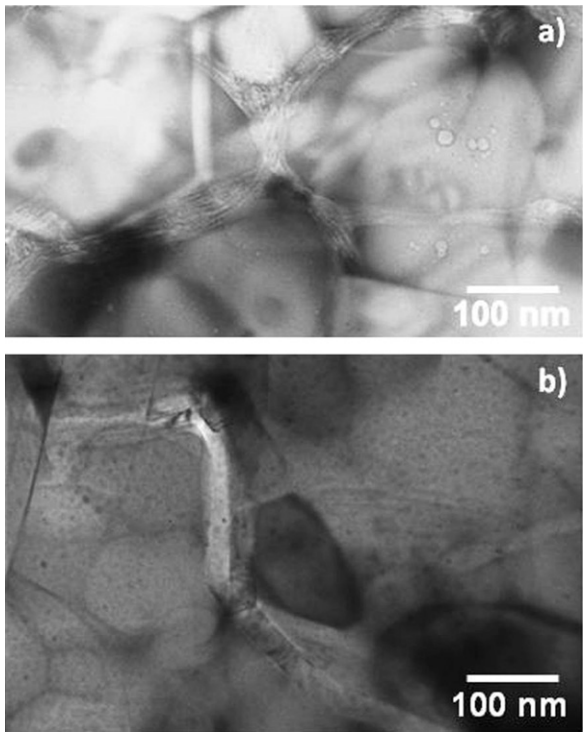

Fig. 6. TEM micrographs of the Si_3N_4 composites containing MWCNTs (a) and GNPs (b) sorrounding the Si_3N_4 grains.

but by the improved inter-GNP contacts in the direction of the SPS pressing axis for higher GNPs contents. This phenomenon would lead to a less resistive GNPs network in that direction, conversely to what happens for nanotubes. The increased number of GNP–GNP contacts would also be responsible for the slightly stronger κ dependence with temperature of this composite compared with other GNPs composites of similar κ values (Fig. 3c).

Provided the intrinsic one- and bi-dimensionality of the MWCNTs and the GNPs, and the observed orientation adjustment of the nanoplatelets during the SPS process (Fig. 2b), a possible anisotropy in the thermal conduction measurements of these specimens cannot be ruled out. In order to ascertain this prospect, we also performed in-plane thermal diffusivity measurements in the direction perpendicular to the SPS pressing axis. From Fig. 5b and c, a clear anisotropic effect is indeed observed for GNPs composites. In particular, the composite containing 16.7 vol. % of nanoplatelets shows through-thickness and in-plane κ values about 0.9 times and twice those of the monolithic material, respectively. These results lead to an enlarged anisotropy of the GNP composites, with $\kappa_{in\text{-}plane}/\kappa_{through\text{-}thickness}$ up to 2.7, compared to the monolithic Si_3N_4, which presented a maximum ratio of 1.3. Conversely, the in-plane thermal conductivity is scarcely modified by the presence of nanotubes. Zhan and Mukherjee[25] also reported no increase for in-plane thermal conductivity of an Al_2O_3 matrix composite. As the through-thickness κ decreases with MWCNTs additions, an increased anisotropy with the MWCNTs content is observed for the MWCNTs/Si_3N_4 materials (Fig. 5c), and then, a slight orientation of MWCNTs bundles

Table 1
Physical properties used for the thermal conductivity calculations of different n-C bulk mats and the ratio between in-plane and through-thickness thermal conductivities.

MATERIAL	P (g cm^{-3})	Φ[a]	α-Through (cm^2 s^{-1})[b]	α-In plane (cm^2 s^{-1}) [b]	$\kappa_{in\text{-}plane}/\kappa_{through}$
Buckypaper	0.5	0.72	0.0056	0.1199	11.9
GNP-602	1.5	0.32	0.0158	0.3292	7.6
GNP-XG	1.8	0.18	0.0283	0.0657	11.6

[a] Φ is porosity fraction calculated using a theoretical density of 1.8 and 2.2 g cm^{-3} for MWCNTs and GNPs, respectively.
[b] α is the experimental thermal diffusivity.

in the network is also inferred to occur during sintering process, although in lesser extent than for GNPs composites. It can be considered that either the contribution of the thermal conduction along nanotubes c axis is higher for heat flowing in the direction perpendicular to SPS pressing axis or less thermal resistive tube–tube contacts exists in that plane, being both phenomena associated to the orientation effect.

In order to confirm that this anisotropy in thermal conduction is related to the orientation of the carbon nanostructures, similar measurements were done in CNTs and GNPs bulk specimens prepared by uniaxial pressing the raw C-n (Fig. 7). The physical properties used for the thermal conductivity calculations of the different C-n bulk materials are given in Table 1. As seen in Fig. 7, thermal conductivity is significantly higher for the GNPs bulk material than for the MWCNTs buckypaper, which can be associated to the presence of large thermal resistances in the later, in agreement with data previously reported in the literature.[1–6] Through-thickness thermal conductivity of the MWCNTs slightly increases with temperature and the κ value at room temperature is relatively low (0.2 W m^{-1} K^{-1}) compared with data reported that are around 20–30 W m^{-1} K^{-1} for unaligned mats of SWCNTs[2–4] and 5–15 W m^{-1} K^{-1} for MWCNTs[5,6] but the density of the present specimen is significantly lower (0.51 g cm^{-3} compared with the reported 1.36 g cm^{-3}). MWCNTs mats showed larger anisotropy than the composites (Fig. 5c), with a thermal conductivity ratio similar to those of the GNPs pressed compacts (Table 1). This confirms that increased tube–tube thermal resistances, as well as a larger contribution of the off-axis thermal

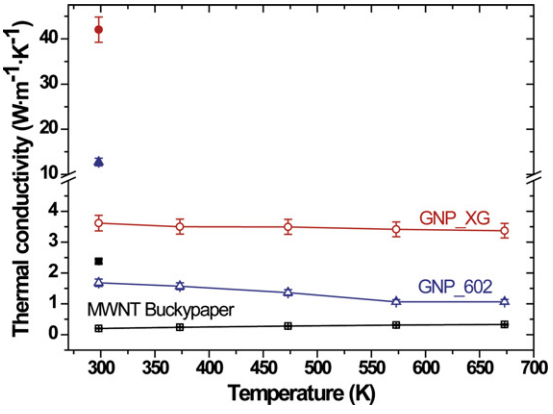

Fig. 7. Through-thickness (open symbols) and in-plane (full symbols) thermal conductivity as a function of temperature of different C-n compacts.

conductivity, occurs in the load direction leading to very low through-thickness κ values and, therefore, explaining the experimental anisotropy observed in the MWCNTs composites. Sinha et al.[41] reported values as low as 1.5 W m^{-1} K^{-1} for the off-axis thermal conductivity of MWCNTs films. A high anisotropy in thermal conductivity (differences of ∼5 times) has also been observed in ultrathin SWCNTs films.[42]

GNPs pressed compacts had higher density (>1.5 g cm^{-3}) than the MWCNTs buckypaper (Table 1) and their through-thickness κ values (Fig. 7) are higher and of the same order of magnitude as those reported for cross-plane pyrolitic graphite[1] (∼5 W m^{-1} K^{-1} at room temperature), and within the range observed for compacted expanded graphite of similar density.[43,44] However, even considering that GNPs might not be perfectly oriented respecting the pressing axis, the in-plane κ values are much lower than it could be expected taking into account that values around 200 W m^{-1} K^{-1} and above 300 W m^{-1} K^{-1} have been reported for polycrystalline graphite[1] and compacted large exfoliated graphite particles,[44] respectively. Therefore, it is evident that thermal resistances associated to GNP–GNP contacts also limit heat conduction in nanoplatelets bulk materials. The larger size nanoplatelets (XG) allow getting compacts with higher density and thermal conductivity than the lower sized GNP (602), which could be explained by a reduction in the number of GNP–GNP contacts. In fact, κ values of graphite has been reported to be strongly limited by a reduced grain size.[1] Considering the GNPs compacts formed by two phases, the porosity and the GNPs network, an estimation of the through-thickness and in-plane thermal conductivities could be done applying the rule of mixtures, giving values of 2.5–4.5 and 20–50 W m^{-1} K^{-1}, respectively. Through-thickness κ values lower than that of the Si_3N_4 matrix and in-plane values higher than the matrix explain that the through-thickness thermal conductivity of the composites slightly decreased with GNPs addition while the in-plane κ significantly increased. Furthermore, in-plane κ values above those measured for the compressed samples were observed for the ceramic composites, indicating that a low thermal resistive GNPs network exists in this plane. A similar anisotropy in the electric response was observed in these composites by contact scanning force microscopy[28] that was also associated to a less resistive network in the graphene plane.

From literature survey[13–25] and present results, the effect of C-n on the through-thickness thermal conductivity of ceramic composites depends on the original thermal conductivity of the matrix, that is, for ceramic with low thermal conductivity, κ

enhancements can be predicted whereas in the case of high conductive ceramics noticeable increases are not to be expected.

4. Conclusions

The addition of carbon nanostructures to Si_3N_4 composites fabricated by spark plasma sintering strongly affects their anisotropic thermal response, which depends on the type of nanostructures. The addition of both carbon nanotubes and graphene nanoplatelets reduces the thermal conductivity in the through-thickness direction leading to an increased anisotropy in ceramic composites. This increase is significantly larger for nanoplatelets additions as it enhances thermal conduction for the in-plane direction up to $40\,W\,m^{-1}\,K^{-1}$, twice the thermal conductivity of the Si_3N_4 matrix. It has been confirmed that the load applied during spark plasma sintering provokes the nanostructures orientation which, jointly to the intrinsic anisotropy in the thermal conductivity of the C-n, leads a less resistive network in the plane perpendicular to the pressing axis.

Acknowledgements

This work was supported by the Spanish Ministry of Science and Innovation (MICINN) and the CSIC under projects number MAT2009-09600 and i-Link 0119, respectively. J. Gonzalez-Julian and C. Ramirez acknowledge the financial support of the JAE (CSIC) fellowship Program. Dr. E. Garcia also acknowledges the financial support of the Ramon y Cajal Program of the MICINN. Experimental supports of S. Molina (ICMM, CSIC) in preparing and viewing GNP/Si_3N_4 transmission specimens and Dr. L.A. Perez Maqueda (IMSE, CSIC) in DSC measurements are acknowledged.

References

1. Baladin AA. Thermal properties of graphene and nanostructured carbon materials. *Nat Mater* 2011;**10**:569–81.
2. Yi W, Lu L, Dian-Lin Z, Pan ZW, Xie SS. Linear specific heat of carbon nanotubes. *Phys Rev B* 1999;**59**:R9015.
3. Hone J, Whitney M, Piskoti C, Zettl A. Thermal conductivity of single-walled carbon nanotubes. *Phys Rev B* 1999;**59**:R2514–6.
4. Hone J, Llaguno MC, Biercuk MJ, Johnson AT, Batlogg B, Benes Z, et al. Thermal properties of carbon nanotubes and nanotube-based materials. *Appl Phys A: Mater Sci Process* 2002;**74**:339–43.
5. Yang DJ, Zhang Q, Chen G, Yoon SF, Ahn J, Wang SG, et al. Thermal conductivity of multiwalled carbon nanotubes. *Phys Rev B* 2002;**66**:165440.
6. Zhang HL, Li JF, Zhang BP, Yao KF, Liu WS, Wang H. Electrical and thermal properties of carbon nanotube bulk materials: experimental studies for 328–958 K temperature range. *Phys Rev B* 2007;**75**:205407.
7. Yu CH, Shi L, Yao Z, Li DY, Majumdar A. Thermal conductance and thermopower of a single-wall carbon nanotubes. *Nano Lett* 2005;**5**:1842–6.
8. Kim P, Shi L, Majumdar A, McEuen PL. Thermal transport measurements of individual multiwalled nanotubes. *Phys Rev Lett* 2001;**87**:215502.
9. Pop E, Mann D, Wang Q, Goodson K, Dai H. Thermal conductance of an individual single-wall carbon nanotube above room temperature. *Nano Lett* 2006;**6**:96–100.
10. Fujii M, Zhang X, Xie H, Ago H, Takahashi K, Ikuta T, et al. Measuring the thermal conductivity of a single carbon nanotube. *Phys Rev Lett* 2005;**95**:065502.
11. Ghosh S, Bao W, Nika DL, Subrina S, Pokatilov EP, Lau CN, et al. Dimensional crossover of thermal transport in few-layer graphene. *Nat Mater* 2010;**9**:555–8.
12. Zhong WR, Zhang MP, Ai BQ, Zheng DQ. Chirality and thickness-dependent thermal conductivity of few-layer graphene: a molecular dynamics study. *Appl Phys Lett* 2011;**98**:113107.
13. Otieno G, Koos AA, Dillon F, Wallwork A, Grobert N, Todd RI. Processing and properties of aligned multi-walled carbon nanotube/aluminoborosilicate glass composites made by sol–gel processing. *Carbon* 2010;**48**:2212–7.
14. Thomas BJC, Shaffer MSP, Boccaccini AR. Sol–gel route to carbon nanotube borosilicate glass composites. *Compos Part A-Appl Sci Manuf* 2009;**40**:837–45.
15. Ning J, Zhang J, Pan Y, Guo J. Fabrication and thermal property of carbon nanotube/SiO_2 composites. *J Mater Sci Lett* 2003;**22**:1019–21.
16. Sivakumar R, Guo S, Nishimurab T, Kagawaa Y. Thermal conductivity in multi-wall carbon nanotube/silica-based nanocomposites. *Scr Mater* 2007;**57**:265–8.
17. Wang HL, Zhou XG, Yu HJ, Zhao S, Luo Z. Property and microstructure of CNTs/AlN ceramics. *Key Eng Mater* 2010;**43**:4–435, 48–49.
18. Datye A, Wu KH, Kulkarni S, Lin HT, Vleugels J, Wenzhi L, et al. Aluminium nitride multiwalled nanotube (MWCNT) nanocomposite by direct in situ growth of CNTs on aluminium nitride particles. *Ceram Eng Sci Proc* 2010;**30**:189–204.
19. Ahmad K, Pan W. Electrical, mechanical, and thermal properties of multi-walled carbon nanotube reinforced alumina composite. *Ceram Eng Sci Proc* 2009;**29**:49–59.
20. Kumari L, Zhang T, Du GH, Li WZ, Wang QW, Datye A, et al. Thermal properties of CNT–Alumina nanocomposites. *Comp Sci Technol* 2008;**68**:2178–83.
21. Tian WB, Kan YM, Zhang GJ, Wang PL. Effect of carbon nanotubes on the properties of ZrB_2–SiC ceramics. *Mater Sci Eng A* 2008;**487**:568–73.
22. Osendi MI, Gautheron F, Miranzo P, Belmonte M. Dense and homogenous silicon nitride composites containing carbon nanotubes. *J Nanosci Nanotechnol* 2009;**9**:6188–94.
23. Corral EL, Wang H, Garay J, Munir Z, Barrera EV. Effect of single-walled carbon nanotubes on thermal and electrical properties of silicon nitride processed using spark plasma sintering. *J Eur Ceram Soc* 2011;**31**:391–400.
24. Koszor O, Lindemann A, Davin F, Balazsi C. Observation of thermophysical and tribological properties of CNT reinforced Si_3N_4. *Key Eng Mater* 2009;**409**:354–7.
25. Zhan GD, Mukherjee AK. Carbon nanotube reinforced alumina-based ceramics with novel mechanical, electrical and thermal properties. *Int J Appl Ceram Technol* 2004;**1**:161–71.
26. De Pablos A, Osendi MI, Miranzo P. Effect of microstructure on the thermal conductivity of hot pressed silicon nitride materials. *J Am Ceram Soc* 2002;**85**:200–6.
27. González-Julián J, Iglesias Y, Caballero AC, Belmonte M, Garzón L, Ocal C, et al. Multi-scale electrical response of silicon nitride/multi-walled carbon nanotubes composites. *Comp Sci Technol* 2011;**71**:60–6.
28. Ramirez C, Garzón L, Miranzo P, Osendi MI, Ocal C. Nanoscale electrical response of new graphene nanoplatelets (GNPs)–Si_3N_4 composites. *Carbon* 2011;**49**:3873–80.
29. González-Julián J, Schneider J, Miranzo P, Osendi MI, Belmonte M. Enhanced tribological performance of silicon nitride-based materials by adding carbon nanotubes. *J Am Ceram Soc* 2011;**94**:2542–8.
30. Belmonte M, González-Julián J, Ramirez C, Schneider J, Osendi MI, Miranzo P. Comportamiento frente al desgaste de materiales compuestos de nitruro de silicio/nanoestructuras de carbono. In: *Proceedings, VI Congreso Iberico de Tribologia 2011*. 2011. p. 5–14.
31. Malek O, Gonzalez-Julian J, Vleugels J, Vanderauwera W, Lauwers B, Belmonte M. Carbon nanofillers for machining insulating ceramics. *Mater Today* 2011;**14**(10):496–501.
32. Gazzara CP, Messier DR. Determination of phase content of Si_3N_4 by X-ray diffraction analysis. *Am Ceram Soc Bull* 1977;**56**:777–80.
33. Donaldson AB, Taylor RE. Thermal diffusivity measurement by a radial heat flow method. *J Appl Phys* 1975;**46**:4584–9.

34. Roine A. Outokumpu HSC Chemistry for Windows V. 5.11. Outokumpu Research: Pori, Finland; 2002.
35. Brito ME, Toriyama M, Kanzaki S. High thermal conductivity in silicon nitride with anisotropic microstructure. *J Am Ceram Soc* 1996;**79**: 2485–8.
36. Belmonte M, Gónzalez-Julián J, Miranzo P, Osendi MI. Spark plasma sintering: a powerful tool to develop new silicon nitride-based materials. *J Eur Ceram Soc* 2010;**30**:2937–46.
37. Hirosaki N, Ogata S, Kocer C, Kitagawa H, Nakamutra Y. Molecular dynamics calculation of the ideal thermal conductivity of single-crystal α- and β-Si_3N_4. *Phys Rev B* 2002;**65**:134110.
38. Hirao K, Watari K, Hayashi H, Kitayama M. High thermal conductivity silicon nitride ceramic. *MRS Bull* 2001;**26**:451–5.
39. Giusca CE, Tison Y, Silva SRP. Evidence for metal-semiconductor transitions in twisted and collapsed double-walled carbon nanotubes by scanning tunneling microscopy. *Nano Lett* 2008;**8**:3350–6.
40. Shi MT, Pettes L. Thermal and structural characterizations of individual single-, double-, and multi-walled carbon nanotubes. *Adv Funct Mater* 2009;**19**:3918–25.
41. Sinha S, Barjami S, Iannacchione G, Schwab A, Muench G. Off-axis thermal properties of carbon nanotube films. *J Nanopart Res* 2005;**7**: 651–7.
42. Li B, Jung HY, Wang H, Kim YL, Kim T, Hahm MG, et al. Ultrathin SWNT films with tunable, anisotropic transport properties. *Adv Funct Mater* 2011;**21**:1810–5.
43. Afanasov IM, Savchenko DV, Ionov SG, Rusakov DA, Seleznev AN, Avdeev VV. Thermal conductivity and mechanical properties of expanded graphite. *Inorg Mater* 2009;**45**:486–90.
44. Bonnissela M, Luob L, Tondeurb D. Compacted exfoliated natural graphite as heat conduction medium. *Carbon* 2001;**39**:2151–61.